

Fast Axial-Scanning Widefield Microscopy With Constant Magnification and Resolution

Manuel Martínez-Corral, Po-Yuan Hsieh, Ana Doblas, Emilio Sánchez-Ortiga, Genaro Saavedra, and Yi-Pai Huang

Abstract—In this paper, we propose the use of electrically-addressable lens devices for performing fast non-mechanical axial scanning when imaging three-dimensional samples. This non-mechanical method can be implemented in any commercial microscope. The approach is based on the insertion of the tunable lens at the aperture stop of the microscope objective. By tuning the voltage, a stack of depth images of 3D specimens can be captured in real time and with constant magnification and resolution. The main advantage of our technique is the possibility of performing fast axial scanning free of mechanical vibrations.

Index Terms—Axial scanning, liquid crystal lens, liquid lens, telecentricity, three-dimensional (3D) microscopy.

I. INTRODUCTION

THREE-DIMENSIONAL (3D) live imaging is important for a better understanding of some biological processes. Although 2D live imaging provides basic dynamic information, such information is often incomplete and, sometimes even misleading since it provides only a partial representation of the 3D biological processes. The ability to study high-speed dynamics of biological functions, or the response of biological systems and tissues to rapid external perturbations, will expand our

knowledge of the biology and may improve our ability to treat injuries.

Current microscopic techniques, like wide-field microscopy [1]–[4], confocal microscopy [1], [3]–[7], structured illumination microscopy [4], [6]–[11] or light-sheet microscopy [12]–[14], are not able to capture with a single shot the 3D structure of a specimen. Instead, the 3D image is obtained computationally after recording a stack of 2D images of different sections within the sample. These images are captured, typically, by mechanical axial scanning of the sample. However, the mechanical movement could damage the sample, or introduce distortions during the recording process due sample vibrations. Besides, mechanical movements slow down the acquisition, which makes impossible the detection of highly-dynamic biological processes,

To avoid the mechanical scanning, one solution is the use of digital holographic microscopy [15]–[17], in which the 3D complex distribution scattered by the sample is directly recorded. This allows the digital refocusing of different sections. Nevertheless, this system operates coherently and makes impossible fluorescence imaging.

Other solutions are the use of a distorted diffraction grating [18] or an off-axis Fresnel lens [19]. With these elements, it is possible to obtain, simultaneously, the image of objects placed at different depths. Notwithstanding, these methods have not been demonstrated in microscopy, and are useful only in case of single 3D scenes composed by isolated elements.

An interesting approach to the task of 3D imaging is the use of an electrically tunable lens (ETL) in order to modify the position of the object plane. In 2010, our Group proposed the use of an ETL for the parallel dynamic focusing of the view images obtained through an array of microlenses [20]. More recently, other groups have applied ETL technology in microscopy. In the case of two-photon scanning microscopy, Grewe *et al.* [21] introduced the ETL in the excitation path of the microscope. Since the focal length of their ETL was always positive, they inserted an offset diverging lens to achieve a symmetrical shifting of the object plane. However, in their system the optical elements were arranged so that the apertures were not matched. As consequence the lateral resolution was significantly worsened and the magnification was different for each plane. The magnification issue was solved by Fahrbach *et al.* [22] by using a telecentric arrangement in a light-sheet microscope. Again the optical power of the ETL was only positive, and therefore an offset diverging lens was required. The main problem of using the offset lens is that in such case it is not possible the perfect

Manuscript received December 24, 2014; revised February 03, 2015; accepted February 10, 2015. Date of publication February 16, 2015; date of current version October 16, 2015. This work was supported in part by the Plan Nacional I+D+I under Grant DPI2012-32994, Ministerio de Economía y Competitividad, Spain, by the Generalitat Valenciana under Grant PROM-ETEOII/2014/072, and by the Ministry of Science and Technology, Taiwan, under Grant 101-2221-E-009-120-MY3. The work of A. Doblas was supported by the University of Valencia through the predoctoral fellowship program “Atracció de Talent”.

A. Doblas, E. Sánchez-Ortiga, G. Saavedra and M. Martínez-Corral are with the 3D Imaging and Display Laboratory, Department of Optics, University of Valencia, E-46100 Burjassot, Spain. (e-mail: A.Isabel.Doblas@uv.es, Emilio.Sanchez@uv.es, Genaro.Saavedra@uv.es, and Manuel.Martinez@uv.es).

P.-Y. Hsieh and Y.-P. Huang are with the Department of Photonic and Display Institutes, National Chiao-Tung University, Taiwan (e-mail: pyhsieh.eo00g@nctu.edu.tw and boundshuang@mail.nctu.edu.tw).

This paper has supplementary material available at <http://www.ieeeexplore.ieee.org>, provided by the author. The supplementary package contains two videos. Media 01.avi shows a stack of depth images obtained with the fast-axial scanning microscope. The scanning is made statically, by shifting the object plane by tuning the voltage of the liquid lens. The object is a cleaning lens tissue paper and the stack covers an axial range of 15 microns. Media 02.avi shows a stack of depth images obtained with the conventional widefield. The scanning is made mechanically, by shifting the object with the help of a micrometer screw. The object is a cleaning lens tissue paper and the stack covers an axial range of 15 microns. The total size of the file is 3.74 MB.

Color versions of one or more of the figures are available online at <http://ieeexplore.ieee.org>.

Digital Object Identifier 10.1109/JDT.2015.2404347

TABLE I
LIST OF ACRONYMS

Acronym	Full name
ETL	Electrically-tunable lens
FFP	Front focal plane
FOV	Field of view
FWHM	Full width at the half maximum
LCL	Liquid crystal lens
LL	Liquid lens
LSI	Linear and shift invariant
MO	Microscope objective
NA	Numerical aperture
PSF	Point spread function
RFP	Rear focal plane
TL	Tube lens

matching of apertures, so that the objective does not work in strict telecentric regime.

As for the confocal case, recently two studies have verified the axial scanning with ETL. Jabbour *et al.* [23] used a single ETL at the detection path of the confocal system. Again the ETL was not placed at the microscope aperture stop, and then the system was resolution- and magnification-variant. In [24], the use of two ETLs, one in the illumination path and the other in the detection path, was proposed. Anyway, regarding confocal microscopy the speed of the axial scanning is not the relevant issue because a full xy scanning is required for any axial scanning step.

In this paper, we state the experimental conditions for obtaining fast axial 3D microscopy with constant magnification, invariant resolution, and symmetrical displacement range. We propose two different electronic devices to face this challenge. First we use a commercially-available liquid lens (LL) [25], [26], and second a liquid-crystal lens (LCL) [27]–[30] that was manufactured by our research team. Specifically we show that the proper use LL permits the axial scanning free of mechanical movements and vibrations. This is important, since it allows speeding up the process and avoiding distortions in the image of dynamic specimens.

The paper is organized as follows. In Section II we describe the theoretical background of wide-field microscopy and the optical method for shifting the object plane. In Section III we present our approach by using either a LL or a LCL. Finally in Section IV we summarize the achievements of this research. Acronyms used in this paper are listed in Table I.

II. BASIC THEORY

Wide-field optical microscopes are arranged by coupling a high numerical aperture (NA) microscope objective (MO) with a low-NA tube lens (TL). The MO is designed to provide high-resolution images free of aberrations for significant field of view (FOV). For this reason the MO are telecentric in the object space, that is, the aperture stop is placed at the rear focal plane (RFP), so that the entrance pupil is at the infinity. It is convenient to couple the MO and the TL in afocal manner (see Fig. 1). In such case, the exit pupil of the arrangement, i.e., the image

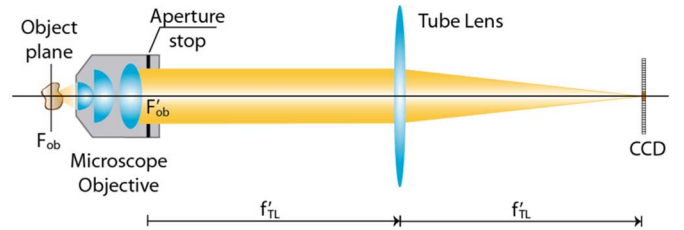


Fig. 1. Scheme of telecentric optical microscope composed by the afocal coupling of the MO and the TL.

of the aperture stop through the TL, is also at the infinite. Under these conditions, the imaging system is said to be strictly telecentric, since it is telecentric in both the object and the image space [31].

Strictly-telecentric arrangements have many advantages over non-telecentric ones. First advantage is that the relation between object distance and image distance is linear,

$$z' = M^2 z \quad (1)$$

where z is the distance between F_{ob} and an object plane and z' the distance between F'_{TL} and the conjugate image plane (usually a microscope is arranged so that $z = z' = 0$). The lateral magnification

$$M = -\frac{f'_{TL}}{f_{ob}} \quad (2)$$

and the axial magnification, M^2 , do not depend on the axial position of the object. The later is a very important issue when thick samples are imaged.

Thanks to their telecentricity, modern optical microscopes are 3D linear and shift invariant (LSI) in amplitude, what implies that it can be defined a 3D amplitude point spread function (PSF). The amplitude PSF can be written, as expressed in the object space, as [1], [4]

$$h(r, z) = -i \frac{2\pi}{\lambda} \int_0^\alpha p(\theta) J_0(kr \sin \theta) e^{ikz \cos \theta} \sin \theta d\theta. \quad (3)$$

In this equation (r, z) are the cylindrical coordinates in the object space, λ is the light wavelength and $k = 2\pi/\lambda$. The aperture angle, α , of the MO is related to its numerical aperture (NA) through $NA = \sin \alpha$, whereas the amplitude transmittance at the aperture stop is represented by function $p(\theta)$. In the usual case of a clear circular aperture, $p(\theta) = 1$. The irradiance PSF is calculated as the squared modulus of (3).

As the first experiment, we measured the irradiance PSF corresponding to a MO with magnification 50x and 0.55 NA (see Fig. 2). As apparent from this experimental result, the telecentricity of the system allows the PSF to be symmetric around the focal plane. The PSF obtained with a widefield microscope, in which no ETL has been inserted, will be named hereafter as the native PSF.

As well known, the MOs are built in such a way that they provide aberration-free images only of objects placed at their FFP. When imaging 3D specimens, the usual procedure is to fix the CCD at the RFP of the TL, and then scan axially the sample.

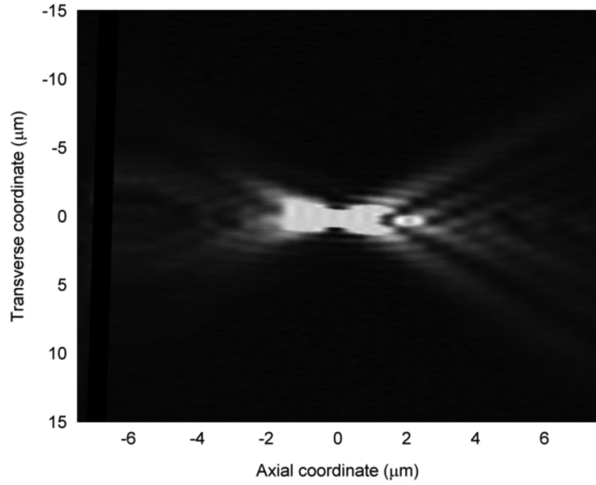


Fig. 2. Experimental measurement of the irradiance PSF of a 50x/0.55 MO. The figure shows a meridian section (x,z) of the irradiance distribution. Detailed explanation of the experimental procedure is given in Section III-A.

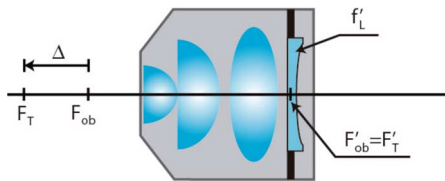


Fig. 3. Scheme of the coupling between a MO and a single lens placed at its RFP.

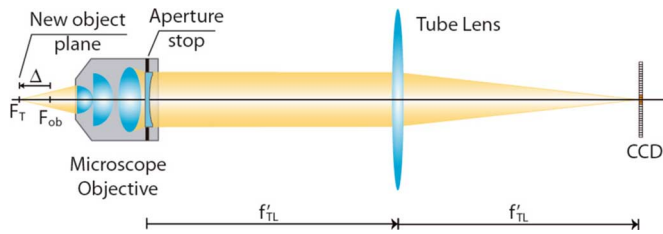


Fig. 4. Scheme of wide-field optical microscope with a single lens inserted at the rear focal plane of the MO.

This allows, for any scan step, the capture an aberration-free 2D image of the corresponding depth section. The stack of acquired 2D images constitutes the 3D image of the sample.

In order to avoid the mechanical displacement of the sample during the axial scanning, a good strategy would be to introduce an element that changes the position of the FFP but keeps invariant the other parameters of the MO. In this sense, our aim here is to introduce in the MO an electrically-addressable optical element that allows the fast axial scanning. The insertion of such element should be made in such way that the telecentricity of the microscope is preserved. To implement this we make use of some elementary concepts of Geometrical Optics. According to them, one can calculate the result of coupling two focal elements so that the second one is a single lens and is placed just at the RFP of the first element, which can be more complex. An example of this situation is shown in the Fig. 3.

For the particular case shown in the Fig. 3, it is easy to show that the focal length, f'_T , of the coupling is equal to the focal length of the MO. The RFP, F'_T , of the coupling remains at the

same position as that of the MO. The only change is found when one calculates the position of the FFP of the coupling, which is displaced by distance

$$\Delta = \frac{f'^2_{MO}}{f'_L} = f'^2_{MO} P_L. \quad (4)$$

In the equation, the optical power, P_L , of the lens is the inverse of its focal length, f'_L . Note that a converging lens produce displacements towards the MO ($\Delta > 0$), and a diverging lens in the opposite direction. In both cases the displacement is proportional to P_L .

From the above information it is apparent that if we insert a, converging or diverging, lens just at the aperture stop of an optical microscope, see Fig. 4, we can modify the position of the object plane, while keeping invariant the lateral magnification of the system and the position of the image plane (still at the CCD).

But the most important issue is that the change is made preserving the telecentric nature of the system. This implies that the system is still 3D LSI and, if the inserted lens does not reduce the effective diameter of the aperture, the amplitude PSF is still calculated by (3), by using the same value of α , and therefore without any worsening of lateral resolution.

III. FAST AXIAL SCANNING SYSTEM

From the theory exposed in the previous section, it is clear that by inserting at the aperture plane an ETL, whose optical power can be tuned by changing the voltage, it is possible to perform a fast axial displacement of the object plane. This controlled displacement will permit to obtain a stack of depth images of thick samples with constant lateral resolution and avoiding any mechanical movement of the sample.

It is desirable to insert the ETL at the aperture stop, which is usually accessible from the backside of the MO [32]. This should be made in such way that the optical axes are adjusted with high accuracy, and also avoiding any reduction in the aperture diameter. To overcome these difficulties in our experiment we inserted in the optical system an afocal relay, Fig. 5. The relay is adjusted so that the FFP of the relay first lens matches the RFP of the MO, whereas the RFP of the second lens matches the FFP of the TL. Proceeding in this way, one makes sure that the same linear combination of plane waves passing through the aperture stop, is also passing, with proportional slope, through the ETL, which is placed at the FFP of the TL.

The use of the afocal relay provides our system with some interesting flexibility, since it permits to match the diameter of the electric lens to that of the aperture stop. For this, one should take into account the relay lateral magnification, $M_{Rel} = -f'_{R2}/f'_{R1}$. We should also take into account that the optical power of the electrical lens is projected onto the aperture stop with a scale factor that depends on the relay system [20],

$$P_{eff} = P_{ETL} M_{Re}^2. \quad (5)$$

Finally, by combination of (4) and (5), we obtain the linear relation

$$\Delta = f'^2_{ob} M_{Re}^2 P_{ETL}. \quad (6)$$

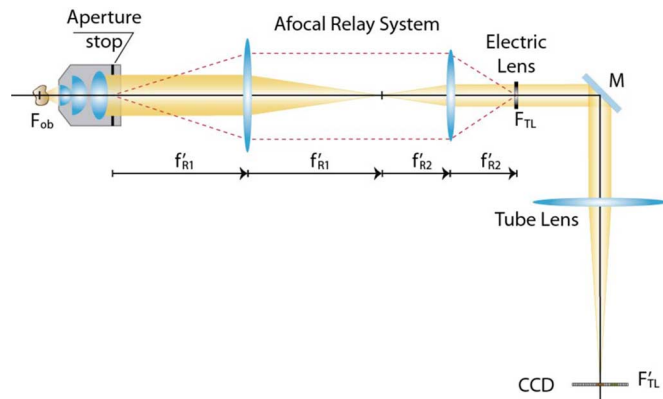


Fig. 5. Scheme of wide-field optical microscope with an ETL inserted in a plane conjugate with the MO aperture stop.

For the implementation of the fast axial wide-field microscope we propose the use of two different ETLs: a liquid lens (LL), and a liquid-crystal lens (LCL).

A. Axial Scanning With a Liquid Lens

To implement our proposal we used first the liquid lens ARCTIC 39N0 manufactured by VARIOPTIC, which is based on electro-wetting technology. The optical power of the lens can be tuned by application of proper electric voltage [25], [26]. The ARTIC 39N0 has a nominal optical aperture of $\phi_{LL} = 3.5$ mm, a maximum wavefront error of 50 nm, and transmission of 97% at $\lambda = 587$ nm. The system does not suffer from hysteresis and the relation between the applied voltage and the induced optical power, in the linear range $[-5.0 \text{ m}^{-1}, +15.0 \text{ m}^{-1}]$, is

$$P_{LL}(T) = S(T)[V - V_0(T)]. \quad (7)$$

Here T is the environmental temperature measured in Celsius ($^{\circ}\text{C}$), and

$$S(T) = 3.1 \times 10^{-5}T^2 - 2.2 \times 10^{-3}T + 1.1. \quad (8)$$

In the particular case of environmental conditions in our laboratory, $S(20) = 1.057$ and $V_0(20) = 45.0$.

1) *Preliminary Experiments*: To make sure of the utility of our proposal, we first measured the transverse irradiance PSF of the microscope for different values of P_{LL} , and compared it with the native PSF. For this experiment we first needed to generate a small focal spot, which acted as the object for the PSF measurement (see Fig. 6). As the light source we used the He-Ne laser beam exiting from an optical fiber with waist $4 \mu\text{m}$. This beam was focused to a small spot by using a large focal length collimating lens ($f'_{CL} = 200$ mm) and a high-NA MO (MO1: $100\times$ and $\text{NA} = 0.90$). As for the optical microscope we used a $50\times/0.55$ MO, a relay with focal lengths $f'_{R1} = 300$ mm and $f'_{R2} = 100$ mm, and a TL of $f'_{TL} = 200$ mm.

After making sure that the small spot was at the FFP of the MO, we recorded the transverse PSF of the native microscope, as shown in Fig. 7(a).

Next, we inserted the liquid lens and, by application of different voltages, obtained the corresponding displacements of the object plane ((6) and (7)). Simultaneously, we displaced mechanically the MO1, to set the focal spot at the MO FFP for

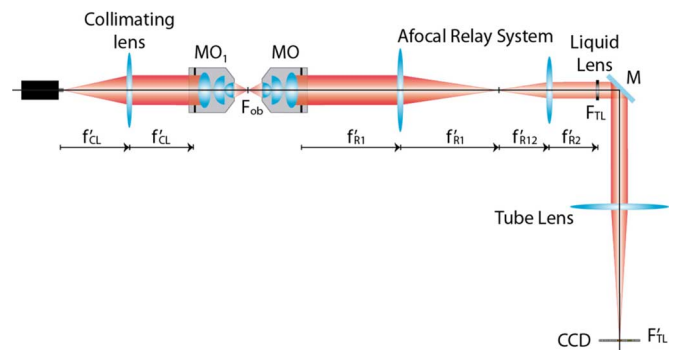


Fig. 6. Scheme system used for the measure of the PSF for different values of P_{LL} . For the measurement of the PSF of the native microscope, the liquid lens was removed.

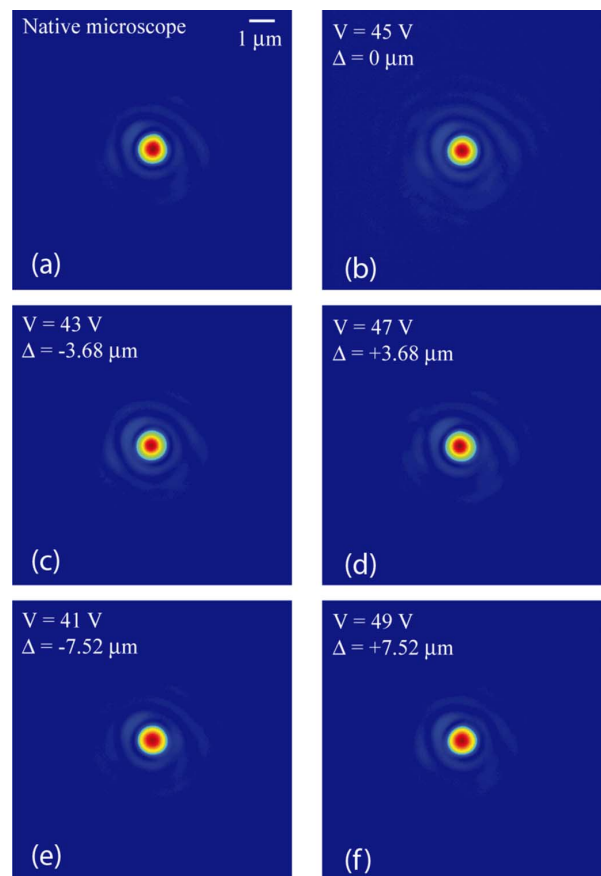


Fig. 7. (a) Measured transverse irradiance PSF, expressed in object space units, of the native microscope; (b)–(f) Measured transverse PSF of the fast-axial microscope for different object-plane positions.

any step of the experiment. Finally, the images were recorded in a 12 bits CCD (EO-5032c, Edmund Optics) with 2448×2048 pixels ($3.75 \mu\text{m}$ width). Next in Fig. 7(b)–(f) we show the results of this. This figure demonstrates that the liquid lens permits the continuous displacement of the object plane with no substantial modification of the PSF. To quantify this similarity, we calculated the correlation coefficient for any of the PSFs in Fig. 7(b)–(f), as compared with the native one [33]. The obtained correlation coefficients are summarized in Table II.

In order to make sure that the transverse resolution is hardly influenced by the use of the liquid lens for the axial scanning we

TABLE II
LIST OF CORRELATION COEFFICIENTS FOR THE TRANSVERSE PSFs OBTAINED WITH THE LIQUID LENS

Voltage (V)	$\Delta(\mu\text{m})$	Correlation coefficient
41.0	-7.52	0.994
43.0	-3.68	0.981
45.0	0	0.981
47.0	+3.68	0.954
49.0	+7.62	0.988

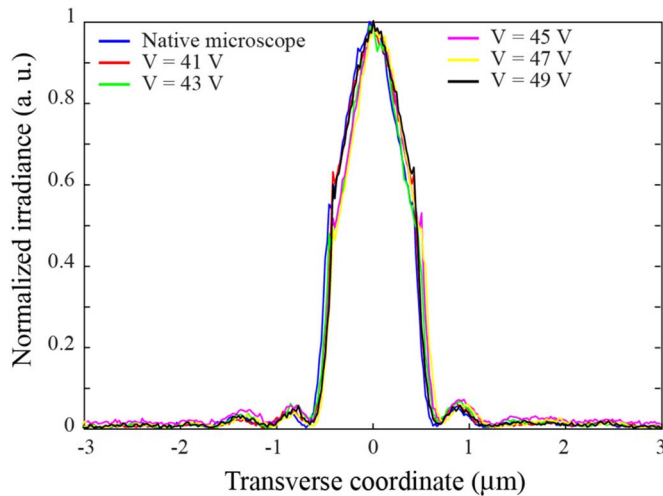


Fig. 8. Irradiance PSFs along the line $y = 0$.

have obtained from the data in Fig. 7 the irradiance PSFs along the line $y = 0$. These PSFs are plotted in Fig. 8. If we use the FWHM as the figure for evaluating the transverse resolution, we find from this figure a variation smaller than 3%.

Finally, prior to the capture of images of fluorescent samples, and aiming to show that the liquid lens hardly introduces significant aberrations in the image, we have measured the 3D irradiance PSF. In case of the native microscope, in absence of liquid lens, we have already shown the PSF in Fig. 2. For making this measurement we have implemented an experimental setup like the one shown in the Fig. 6 (but without the liquid lens), and have made the axial scanning by displacing the MO1.

In case of the fast-axial microscope, we inserted the liquid lens at the position shown in Fig. 6, and made the axial scanning by tuning the voltage of the liquid lens, while keeping static the CCD. The results of this measurement are shown in Fig. 9. The results obtained with both microscopes are again very similar. To evaluate the similarity between them, we calculated the correlation coefficient and obtained a value of 0.93. This high value permits to state that the insertion of the LL hardly introduces significant aberrations.

2) *Imaging Experiments*: Once we have verified that the liquid lens permits the fast displacement of the object plane with no significant worsening of transverse, or even 3D, irradiance PSF, we performed an imaging experiment in which we obtained a stack of depth section of a microscopic thick sample. In our experiment we used as the sample a cleaning-lens tissue paper. These sheets are made for cleaning the lenses of high-quality optical instruments, but are also commonly used

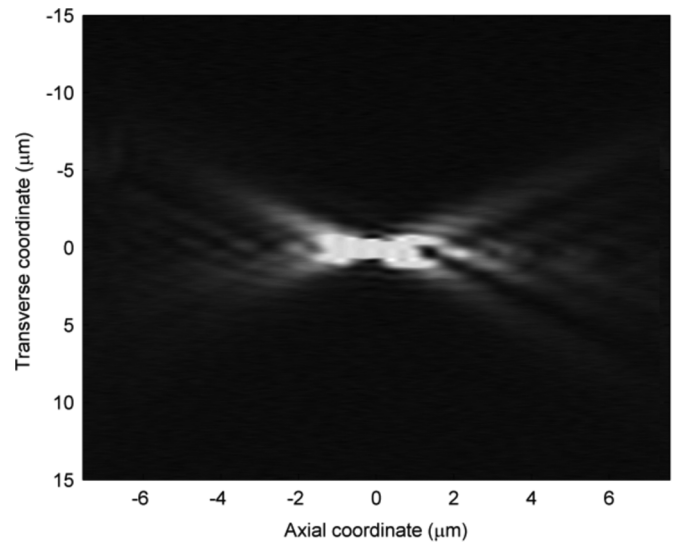


Fig. 9. Experimental measurement of the irradiance PSF of a microscope equipped with a 50x/0.55 MO, and an ARTIC 39N0 liquid lens. The figure shows a meridian section (x,z) of the irradiance distribution.

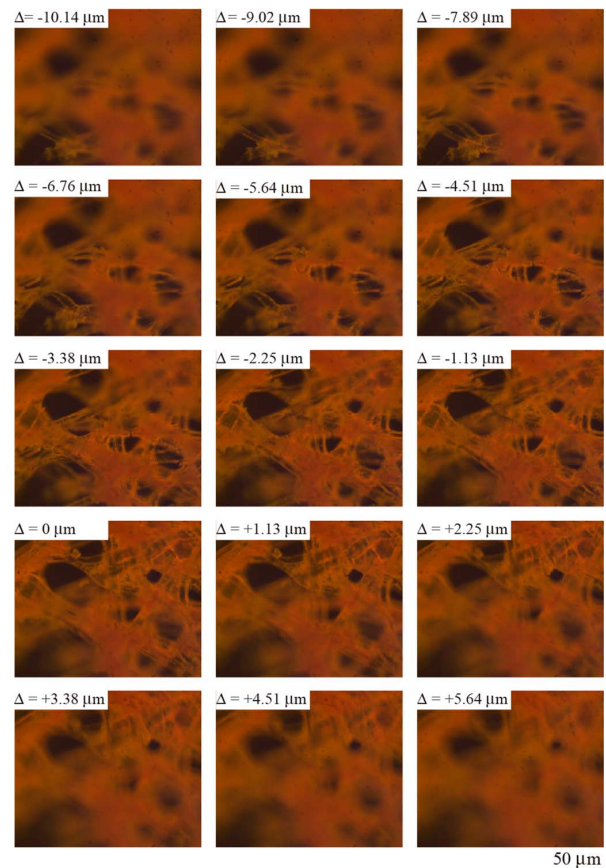


Fig. 10. Stack of depth images obtained with the fast-axial scanning microscope. These images are mounted in a video (Media 1).

in testing microscopy experiments. They have low-density of threads, and about 100 microns of thickness. In our experiment the tissue was stained with fluorescent ink proceeding from a stabile highlighter. The sample was illuminated with the uniform beam proceeding from an ultrabright green LED with

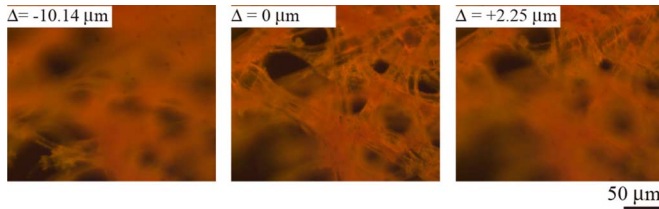


Fig. 11. Three depth images obtained with the conventional microscope when displacing the sample mechanically. These images, together with other intermediate images, are mounted in a video (Media 2).

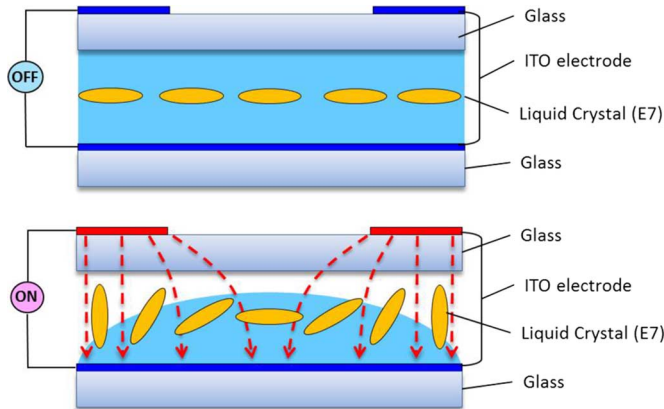


Fig. 12. Cross-section of a LCL device. The electric fringing field induces a lens-like refractive index variation inside the liquid crystal cell.

emission central wavelength at 460 nm and with 20 nm of spectral FWHM. The experimental setup was the one schematized in Fig. 5. Next, in Fig. 10, we show the set of equidistant depth images obtained with the fast-axial microscope.

The scanning range of the fast-axial microscope can be easily calculated with (6) and is of $\Delta_{\max} = 36 \mu\text{m}$. If the LL were inserted directly at the RFP of the MO (without need of any relay system) the scanning range would be calculated with (4) and be of $\Delta_{\max} = 320 \mu\text{m}$.

The synchronized axial displacement, shooting and recording of the elemental images was controlled by a LabVIEW® code. The complete sequence of 18 depth images was obtained in 0.78 seconds, and with no need of any mechanical displacement. In fact the main limitation in acquisition speed is imposed by the CCD frame rate (which in our case was 24 frames/second), since the response speed of the ARTIC 39N0 is of 9 ms. A proper selection of the CCD could produce an acquisition speeds up to 100 depth images per second.

To illustrate the accuracy of our proposal, we also obtained the images of three of the above sections, but with the microscope mounted in the conventional configuration (without LL) and displacing the sample mechanically. The images are shown in Fig. 11. It is apparent that the images obtained with the proposed fast-axial microscope have, essentially, the same contrast, FOV and resolution than the ones obtained with the conventional native microscope.

B. Axial Scanning With a Liquid-Crystal Lens

As second approach, we used an electric-field-driven liquid crystal lens (LCL) [34] for the implementation of our fast-axial

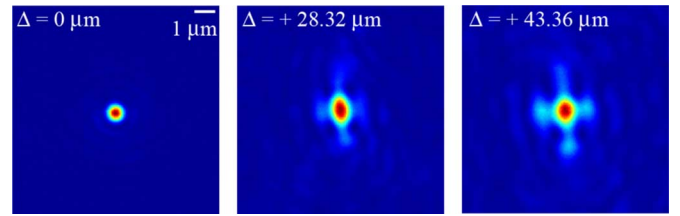


Fig. 13. PSF of the fast axial microscope with LC-lens for different positions of the object plane.

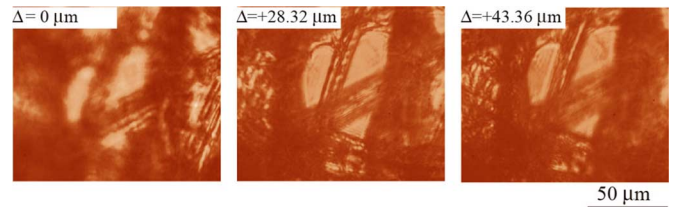


Fig. 14. Stack of depth images obtained with a LCL device inserted in a wide-field microscope.

TABLE III
DOUBLE-LAYER LCL. APPLIED VOLTAGES AND SUBSEQUENT OPTICAL POWERS AND AXIAL DISPLACEMENTS

Voltage (V)	P_{LCL} (m^{-1})	P_{eff} (m^{-1})	Δ (μm)
0/0	0	0	0
25/0	11.5	1.28	20.44
25/25	15.9	1.77	28.32
50/50	24.4	2.71	43.36

scanning microscope. Different to LL technology, the lens effect of LCL is based on the phase delay between the center and the edge of lens aperture (Fig. 12). By applying electric voltage on the ITO (Indium Tin Oxide) electrode of LCL, the liquid crystal molecule will be arranged along the fringing electric field from the ITO electrodes and it will induce a lens-like variation of the effective refractive index in the homogeneous liquid crystal cell.

The LCL was built by our Group, in Taiwan Lab., and has a nominal optical diameter of $\phi = 2r = 2 \text{ mm}$, and cell gap of $d = 60 \mu\text{m}$. The liquid crystal material is E7, which has an ordinary refractive index of $n_o = 1.5183$ and an extraordinary refractive index of $n_e = 1.7371$. The maximum lens power can be calculated as

$$P_{LCL} = 2\Delta n \frac{d}{r^2}. \quad (9)$$

In the experiments, we used a double layer liquid crystal device both with $60 \mu\text{m}$ cell gap to induce larger optical powers. Specifically, the effective optical power of the double-layer LCL can be tuned in the range $[0, +24.4 \text{ m}^{-1}]$ as shown in Table III. As in Section III-A, first we performed a preliminary experiment with the aim of measuring the microscope PSF for different values of P_{LCL} . Using the same experimental setup, sketched in Fig. 6, we obtained the results shown in Fig. 13. The obtained PSFs are much worse than the ones provided by both the native microscope ($\Delta = 0 \mu\text{m}$) and the LL technology. Next, Fig. 14 shows the depth images of a lens tissue obtained by the

LCL device. From this figure, it is clear that the object plane is axially shifted, but the image quality and contrast ratio are not acceptable. Note however that this technology is currently in its initial stage and therefore fast improvements are expected in the forthcoming years. It is then reasonable to guess the production of LCL with non-distorted PSF and faster response. This could be made with high-resistance LCL [35], [36] or polymer-layer LCL [37], [38]. Other drawback, at the current stage of development, is the slow response time of LCL, which depends on the LC thickness, ranging from 200 to 500 ms. The main advantages of LCL technology are its thinner volume and lighter weight. For these reasons, LCL should also be, in the next few years, a good candidate for a tunable MO for fast axial 3D wide-field microscopy.

IV. CONCLUSION

In summary, we have shown the goodness of ETL technology to produce non-mechanically the axial scanning of 3D samples in optical microscopy. The method consists of the insertion of an ETL at the aperture stop of a MO. If such insertion was made by the MO manufacturer, the proposed technique could be easily implemented in commercial microscopes. By applying the proper voltage, the focal length of the device gradually changes and then different sections of the specimen are focused in real time. Our method has been validated with experimental results by using an LL and an LCL. Specifically, for the case of the LL, we have demonstrated, for the first time we believe, the invariance of the resolution over the axial scanning range. We have obtained a symmetrical displacement range without any offset lens. Besides, our results exhibit higher resolution than previously reported. Regarding the LCL technology, we have to recognize that at present it is not able to produce an axial scanning with reasonable speed and image quality. However, this technology is experiencing a rapid development and soon will be providing promising results.

REFERENCES

- [1] Gu, *Advanced Optical Imaging Theory*. New York, NY, USA: Springer, 1999.
- [2] D. B. Murphy, *Fundamentals of Light Microscopy and Electronic Imaging*. New York, NY, USA: Wiley-Liss, 2001.
- [3] J. B. Pawley, *Handbook of Biological Confocal Microscopy*, 3rd ed. New York, NY, USA: Springer, 2006.
- [4] M. Martínez-Corral and G. Saavedra, "The resolution challenge in 3D optical microscopy," *Progress in Optics*, vol. 53, pp. 1–68, 2009.
- [5] M. Gu and C. J. R. Sheppard, "Confocal fluorescent microscopy with a finite-sized circular detector," *J. Opt. Soc. Amer. A*, vol. 9, pp. 151–153, 1992.
- [6] T. Wilson, *Confocal Microscopy*. New York, NY, USA: Academic, 1990.
- [7] E. Sánchez-Ortiga, C. J. R. Sheppard, G. Saavedra, M. Martínez-Corral, A. Doblas, and A. Calatayud, "Subtractive imaging in confocal scanning microscopy using a CCD camera as a detector," *Opt. Lett.*, vol. 37, pp. 1280–1282, 2012.
- [8] M. A. A. Neil, R. Juskaitis, and T. Wilson, "Method of obtaining optical sectioning by using structured light in a conventional microscope," *J. Opt. Soc. Amer. A*, vol. 22, pp. 1905–1907, 1997.
- [9] M. G. L. Gustafsson, "Surpassing the lateral resolution by a factor of two using structured illumination microscopy," *J. Microsc.*, vol. 198, pp. 82–87, 2000.
- [10] M. G. L. Gustafsson *et al.*, "Three-dimensional resolution doubling in wide-field fluorescence microscopy by structured illumination," *Biophysical J.*, vol. 94, pp. 4957–4970, 2008.
- [11] A. G. York *et al.*, "Resolution doubling in live, multicellular organisms via multifocal structured illumination microscopy," *Nature Methods*, vol. 9, pp. 749–754, 2013.
- [12] A. H. Voie, D. H. Burns, and F. A. Spelman, "Orthogonal-plane fluorescence optical sectioning: Three-dimensional imaging of macroscopic biological specimens," *J. Microscopy*, vol. 170, pp. 229–236, 1993.
- [13] E. H. K. Stelzer, K. Greger, and E. G. Reynaud, *Light Sheet Based Fluorescence Microscopy: Principles and Practice*. New York, NY, USA: Wiley-Blackwell, 2014.
- [14] P. A. Santi, "Light sheet fluorescence microscopy: A review," *J. Histochem Cytochem*, vol. 59, pp. 129–138, 2011.
- [15] I. Moon and B. Javidi, "Three-dimensional identification of stem cells by computational holographic imaging," *J. R. Soc. Interface*, vol. 4, pp. 305–313, 2007.
- [16] E. Sánchez-Ortiga, P. Ferraro, M. Martínez-Corral, G. Saavedra, and A. Doblas, "Digital holographic microscopy with pure optical spherical phase compensation," *J. Opt. Soc. Amer. A*, vol. 28, pp. 1410–1417, 2011.
- [17] P. Picart and J. C. Li, *Digital Holography*. Hoboken, NJ, USA: Wiley, 2012.
- [18] P. M. Blanchard and A. H. Greenaway, "Simultaneous multiplane imaging with a distorted diffraction grating," *Appl. Opt.*, vol. 38, pp. 6692–6699, 1999.
- [19] S. Djidel, J. K. Gansel, H. I. Campbell, and A. H. Greenaway, "High-speed, 3-dimensional, telecentric imaging," *Opt. Express*, vol. 14, pp. 8269–8277, 2006.
- [20] A. Tolosa, R. Martínez-Cuenca, A. Pons, G. Saavedra, M. Martínez-Corral, and B. Javidi, "Optical implementation of micro-zoom arrays for parallel focusing in integral imaging," *J. Opt. Soc. Amer. A*, vol. 27, pp. 495–500, 2010.
- [21] B. F. Grewe, F. F. Voigt, M. van't Hoff, and F. Helmchen, "Fast two-layer two-photon imaging of neural cell populations using an electrically tunable lens," *Biomed. Opt. Express*, vol. 2, pp. 2035–2046, 2011.
- [22] F. O. Fahrbach, F. F. Voigt, B. Schmid, F. Helmchen, and J. Huisken, "Rapid 3D light-sheet microscopy with a tunable lens," *Opt. Express*, vol. 21, pp. 21010–21026, 2013.
- [23] J. M. Jabbour *et al.*, "Optical axial scanning in confocal microscopy using an electrically tunable lens," *Biomed. Opt. Express*, vol. 5, pp. 645–652, 2014.
- [24] N. Koukourakis *et al.*, "Axial scanning in confocal microscopy employing adaptive lenses (CAL)," *Opt. Express*, vol. 22, pp. 6025–6039, 2014.
- [25] C. Quillet and B. Berge, "Electrowetting: A recent outbreak," *Curr. Opin. Colloid Interface Sci.*, vol. 6, pp. 34–39, 2001.
- [26] B. Berge and J. Peseux, "Variable focal lens controlled by an external voltage: An application of electrowetting," *Eur. Phys. J. E*, vol. 3, pp. 59–163, 2000.
- [27] S. Sato, "Liquid-crystal lens-cells with variable focal length," *Jpn. J. Appl. Phys.*, vol. 18, pp. 1679–1684, 1979.
- [28] H. Ren, D. W. Fox, B. Wu, and S. T. Wu, "Liquid crystal lens with large focal length tunability and low operating voltage," *Opt. Express*, vol. 15, pp. 11328–11335, 2007.
- [29] H. Ren, Y. H. Fan, S. Gauza, and S. T. Wu, "Tunable-focus cylindrical liquid crystal lens," *Jpn. J. Appl. Phys.*, vol. 43, pp. 652–653, 2004.
- [30] Y. P. Huang, C. W. Chen, and Y. C. Huang, "Superzone fresnel liquid crystal lens for temporal scanning auto-stereoscopic display," *J. Display Technol.*, vol. 8, no. 11, pp. 650–655, Nov. 2012.
- [31] M. Born and E. Wolf, *Principles of Optics*. Oxford, U.K.: Pergamon, 1980.
- [32] R. Juskaitis, "Characterizing high-NA microscope objective lenses," in *Optical Imaging and Microscopy: Techniques and Advanced Systems*, P. Török and F. J. Kao, Eds. New York, NY, USA: Springer-Verlag, 2003.
- [33] The correlation coefficient is calculated by using the MatLab function "corr2". Basically this function calculates correlation between the native PSF and the fast-axial PSF, divided by the self correlation of the native PSF. Both correlations are evaluated at the origin.
- [34] H. Hong, S. Jung, B. J. Lee, and H. H. Shin, "Electric-field-driven LC lens for 3-D/2-D autostereoscopic display," *J. Soc. Inf. Display*, vol. 17, pp. 399–406, 2009.
- [35] L. Y. Liao, Y. P. Huang, Y. M. Lin, and H. P. Shieh, "Liquid crystal lens and manufacturing method thereof," U.S. Patent 8345194 B2, Jan. 1, 2013.
- [36] Y. C. Chang, T. H. Jen, C. H. Ting, and Y. P. Huang, "High-resistance liquid crystal lens array for rotatable 2D/3D auto-stereoscopic display," *Opt. Express*, vol. 22, pp. 2714–2724, 2014.

- [37] T. Nose, S. Masuda, S. Sato, J. Li, L. C. Chien, and P. J. Bos, "Effects of low polymer content in a liquid-crystal microlens," *Opt. Lett.*, vol. 22, pp. 351–353, 1997.
- [38] Y. H. Fan, H. Ren, and S. T. Wu, "Switchable fresnel lens using polymer-stabilized liquid crystals," *Opt. Express*, vol. 11, pp. 3080–3086, 2003.



Manuel Martinez-Corral was born in Spain in 1962. He received the M.Sc. and Ph.D. degrees in physics from the University of Valencia in 1988 and 1993, respectively.

He is currently Full Professor of Optics at the University of Valencia, where he is co-leader of the "3D Imaging and Display Laboratory". His research interest includes resolution procedures in 3D microscopy, and 3D imaging and display technologies. He has supervised on these topics ten Ph.D. theses, two of them honored with the Ph.D. Extraordinary

Award. He has published over 80 technical articles in major journals, and pronounced over 30 invited and 5 keynote presentations in international meetings.

Dr. Martinez-Corral has been member of the Scientific Committee in over 15 international meetings, and was the president of the Organizing Committee of the international conference Focus on Microscopy 2007. He is co-chair of the Three-Dimensional Imaging, Visualization, and Display Conference within the SPIE meeting in Defense, Security, and Sensing (Baltimore). He is Topical Editor of the IEEE/OSA JOURNAL OF DISPLAY TECHNOLOGY. In 1993, the University of Valencia honored him with the Ph.D. Extraordinary Award. In 2010, he was named Fellow of the SPIE.



Po-Yuan Hsieh received the B.Sc. and M.Sc. degrees from the Department of Photonics, National Chiao-Tung University, Taiwan, in 2009 and 2011, respectively, and is currently working toward the Ph.D. degree.

His research interests include Liquid Crystal devices, 3D image capturing, and 3D image processing.



Ana Doblas was born in Spain in 1987. She received the B.Sc. and M.Sc. degrees in physics from the University of Valencia, Spain, in 2010 and 2011, respectively, and is currently working toward the Ph.D. degree at the same university.

Since 2009, she has been working with the 3D Imaging and Display Laboratory (University of Valencia), where she is currently running her Ph.D. project and holds a pre-doctoral fellowship. Her research interests include 3D optical microscopy and image formation theory.



Emilio Sánchez-Ortiga received the M.Sc. and Ph.D. degrees in physics from the University of Valencia, Spain, in 2009 and 2014, respectively.

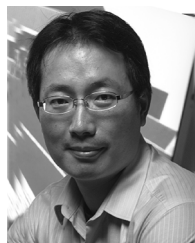
He has published 11 manuscripts in major journals, and authored over 30 communications in scientific conferences. He is currently holding a postdoctoral contract in the University of Valencia. His main research topic is 3D microscopy, including confocal scanning microscopy, structured illumination microscopy and digital holographic microscopy.



Genaro Saavedra received the B.Sc. and Ph.D. degrees in physics from Universitat de València, Spain, in 1990 and 1996, respectively. His Ph.D. work was honored with the Ph.D. Extraordinary Award.

He is currently an Associate Professor with this University. Since 1999, he has been working with the "3D Display and Imaging Laboratory", at the Optics Department. His current research interests are optical diffraction, integral imaging, 3D high-resolution optical microscopy and phase-space representation of scalar optical fields. He has published on these

topics about 50 technical articles in major journals and 3 chapters in scientific books. He has published over 50 conference proceedings, including 10 invited presentations.



Yi-Pai Huang received the B.S. degree from National Cheng Kung University in 1999, and the Ph.D. degree in electro-optical engineering at the National Chiao Tung University, Hsinchu, Taiwan, in 2004.

In 2004, he was a project leader in the technology center of AU Optronics (AUO), and was a visiting associate professor of Cornell University, Ithaca, NY, USA, in 2011. He is currently a full-time professor in the Department of Photonics and Display Institute at National Chiao Tung University, Hsinchu, Taiwan.

His expertise includes 3d display and interactive technologies, display optics and color science, micro-optics. In the above-mentioned research, he has so far published more than 40 International Journal papers articles with more than 110 international conference papers (including the 25 Invited presentations), and has obtained about 70 patents.

Dr. Huang received the SID's distinguished paper award three times (2001, 2004, 2009) and the *J. SID* Best Paper of the Year Award in 2010. Other important awards include 2013 Outstanding Chinese Youth Engineering Award, 2012 National Youth Inventor Award of Economic Affairs, 2011 Taiwan National Award of Academia Inventor, 2010 Advantech Young Professor Award. Furthermore, he is also currently the General Director of Taiwan 3D Interaction & Display Association (3DIDA), the Chairman of Society of Information Display Taipei chapter (SID-Taipei).